scientific reports



OPEN Toward real-time margin assessment in breast-conserving surgery with hyperspectral imaging

Lynn-Jade S. Jong^{1,2}, Dinusha Veluponnar^{1,2}, Freija Geldof¹, Joyce Sanders³, Marcos Da Silva Guimaraes³, Marie-Jeanne T. F. D. Vrancken Peeters¹, Frederieke van Duijnhoven¹, Henricus J. C. M. Sterenborg¹, Behdad Dashtbozorg^{1⊠} & Theo J. M. Ruers^{1,2}

Margin assessment in breast-conserving surgery (BSC) remains a critical challenge, with 20-25% of cases resulting in inadequate tumor resection, increasing the risk of local recurrence and the need for additional treatment. In this study, we evaluate the diagnostic performance of hyperspectral imaging (HSI) as a non-invasive technique for assessing resection margins in ex vivo lumpectomy specimens. A dataset of over 200 lumpectomy specimens was collected using two hyperspectral cameras, and a classification algorithm was developed to distinguish between healthy and tumor tissue within margins of 0 and 2 mm. The proposed approach achieved its highest diagnostic performance at a 0 mm margin, with a sensitivity of 92%, specificity of 78%, accuracy of 83%, Matthews correlation coefficient of 68%, and an area under the curve of 89%. The entire resection surface could be imaged and evaluated within 10 minutes, providing a rapid and non-invasive alternative to conventional margin assessment techniques. These findings represent a significant advancement toward real-time intraoperative margin assessment, highlighting the potential of HSI to enhance surgical precision and reduce re-excision rates in BCS.

Keywords Breast-conserving surgery, Hyperspectral imaging, Resection margin assessment, Breast tissue, Tissue classification

Breast cancer remains a global health concern with an annual incidence of more than 2.2 million newly diagnosed cases worldwide, ranking as the leading cause of cancer among women¹. To treat this disease, breast-conserving surgery (BCS) is often conducted followed by radiotherapy with the primary objective of only resecting the tumor while keeping surrounding healthy tissue intact, ensuring the most favorable cosmetic result possible. To achieve optimal patient outcomes following BCS, the evaluation of resection margins stands as a critical factor during the surgical procedure²⁻⁵. However, aiming for clear margins remains challenging as surgeons are limited to visual and tactile feedback, increasing the complexity of such procedures when the tumor is not visible or palpable. In complex cases when the tumor cannot be identified properly, surgeons can decide to conduct a traditional frozen section analysis to assess the surgical margin status intraoperatively.

While this technique allows for accurate analysis of breast surgical margins, its drawback lies in its timeconsuming nature and restriction to examine only a small fraction of the entire lumpectomy resection surface⁶. This limitation may result in overlooking critical regions that could be positive for tumor tissue. Consequently, surgeons continue to depend on the gold standard for a thorough evaluation of surgical margins. This gold standard involves histopathological examination, a process that often requires several days. Due to the prolonged histopatholgical processing time (2-5 days) and lack of adequate margin assessment during surgery, surgical margins still remain tumor-positive in about 20-25% of the cases depending upon adherence to national oncology guidelines⁷⁻¹². Therefore, there is a need for advanced real-time technologies to assist surgeons in the evaluation of surgical margins during surgery. Such technologies would allow immediate re-excision of any suspected areas, reducing the number of ultimate tumor-positive margins and thereby decreasing the necessity for additional treatment, which negatively impacts quality of life and increases healthcare expenses.

¹Image-Guided Surgery, Department of Surgery, Netherlands Cancer Institute, Plesmanlaan 121, Amsterdam 1066 CX, The Netherlands. ²Faculty of Science and Technology, University of Twente, Drienerlolaan 5, Enschede 7522 NB, The Netherlands. ³Department of Pathology, Netherlands Cancer Institute, Plesmanlaan 121, Amsterdam 1066 CX, The Netherlands. [™]email: b.dasht.bozorg@nki.nl

To address these challenges, various alternative approaches are being explored ^{13,14}, including intraoperative ultrasonography ^{15,16}, radiofrequency ¹⁷⁻²⁰ and bioimpedance spectroscopy ²¹, Raman spectroscopy ²²⁻²⁴, diffuse reflectance spectroscopy ^{25,26}, digital breast tomosynthesis ²⁷, fluorescence imaging ²⁸, microcomputed tomography ²⁹, optical coherence tomography ³⁰⁻³², ultraviolet photoacoustic microscopy ³³, intraoperative flow cytometry ^{34,35}, and microscopy with ultraviolet surface excitation ³⁶. While some of these techniques show promise, none have yet been adopted into routine clinical practice. Barriers to implementation include limited diagnostic accuracy, time-consuming procedures, complex interpretation, operator dependence, incomplete margin coverage, early-stage development, and uncertain cost-effectiveness.

Hyperspectral imaging (HSI) is an optical imaging technique, which has the potential to address this challenge and fulfil the clinical needs from surgeons. Unlike many other optical or imaging methods, HSI offers unique advantages. It is a fast, non-contact, and non-invasive technique that does not rely on contrast agents and is free from radiation exposure. With its ability to capture data from the reflected light of entire tissues across a wide range of wavelengths - far beyond what the human eye can perceive - HSI has proven to be a promising tool for different clinical applications, for example oxygen saturation assessment^{37–39}, blood vessel detection^{40,41}. Additionally, HSI has been investigated for margin assessment during cancer surgery^{42–66}.

In previous studies conducted by our research group, we specifically explored the use of hyperspectral imaging for margin assessment in breast-conserving surgery 45,46,48,67,68. In these studies, we initially explored the use of HSI under highly controlled conditions. A dataset of gross-sectioned breast tissue slices was acquired and used to develop a tissue classification algorithm to distinguish between healthy and tumor tissue^{45,46}. Following the excellent performance of this algorithm, we transitioned to studying lumpectomy specimens that had not yet undergone histopathological processing, thereby representing the actual resection surface during surgery. This feasibility study, involving only six lumpectomy specimens faced significant limitations⁴⁵. The primary challenge was correlating the hyperspectral data with histopathology due to the limited available histopathologic information, preventing a comprehensive evaluation of the entire imaged resection surface. Furthermore, discrepancies were noted between breast tissue slices and lumpectomy specimens in terms of tissue thickness, freshness, surface structure, blood saturation, and cauterization. These differences made it challenging to directly apply the developed classification algorithm from tissue slices to lumpectomy resection surfaces⁴⁸ Additionally, the complexity of correlating hyperspectral data with histopathology had to be addressed before advancing. To this end, we successfully developed a novel hyperspectral-unmixing-based approach on lumpectomy specimens to accurately assign ground-truth labels to hyperspectral images and created a robust classification algorithm. At that stage, the classification performance was only evaluated at various locations on a single lumpectomy resection side⁶⁸.

In the current study, we build upon our previous research with a focused objective: to employ HSI for the comprehensive evaluation of the entire resection surface of lumpectomy specimens.

We specifically address the limitations observed in earlier studies and highlight our main contributions:

- Tissue structure and thickness: Measurements were taken directly from the original resection surface, ensuring realistic variations in tissue structure and thickness compared to grossly sectioned tissue slices
- Freshness: Unlike previous studies using processed specimens, we acquired hyperspectral data immediately after surgery, preserving the natural tissue characteristics as much as possible
- Cauterization: Since data collection occurred after surgery, it included the cauterization effects introduced during the procedure
- Large-scale dataset: We used a dataset of over 200 patients, improving algorithm robustness
- Comprehensive evaluation: We examined the entire resection surface instead of limited regions
- Diagnostic performance: In contrast to previous studies, which either only confirmed malignancies using available H&E sections without assessing diagnostic performance or evaluated it in limited regions, we assess both sensitivity and specificity of hyperspectral imaging across the entire resection surface to determine the surgical margin status

These contributions represent a critical step toward the final clinical application, aiming to provide surgeons with a real-time tool for assessing resection margins during BCS.

Materials and methods Study design

This study was conducted between 2018 and 2021 at the Netherlands Cancer Institute - Antoni van Leeuwenhoek Hospital (NKI-AVL). This study is approved by the NKI-AVL Institutional Review Board of the hospital (protocol code CFMPB545) and adheres to the Declaration of Helsinki. Informed consent was obtained from all patients and/or their legal guardians in accordance with the Dutch Medical Research Involving Human Subjects Act (WMO), allowing the use of their tissue samples in this study. In total, a dataset on *ex vivo* lumpectomy specimens was collected from 204 female patients with breast cancer who underwent primary breast-conserving surgery at the Netherlands Cancer Institute-Antoni van Leeuwenhoek hospital. The lumpectomy specimens of patients who had neoadjuvant therapy were also included. The lumpectomy specimens of the patients undergoing a reoperation were excluded from this study. Immediately after excision, the lumpectomy specimens were measured with hyperspectral cameras that were situated within the operating room facility. Following the optical measurements, the lumpectomy specimens were transported to the pathology department where they were processed according to standard protocol.

Hyperspectral camera systems

The lumpectomy specimens were measured using two line-scanning hyperspectral cameras (Specim, Spectral Imaging Ltd., Oulu, Finland), selected for their high spatial and spectral resolution, which provides detailed imaging and enhanced tissue type discrimination. The first camera (PFD-CL-65-V10E) features a CMOS sensor with 1312×384 pixels, capturing 384 wavelength bands at 3 nm increments in the visible (VIS) region (400-1000 nm) with a spatial resolution of 0.16 mm per pixel. The second camera (VLNIR CL-350-N17E) uses an InGaAs sensor with 320×256 pixels, offering 256 wavelength bands at 5 nm increments in the near-infrared (NIR) region (900-1700 nm) and a spatial resolution of 0.5 mm per pixel. These cameras' broad wavelength range, including the NIR spectrum, minimizes the impact of blood/hemoglobin absorption, allowing for more accurate capture of relevant chromophores. The geometry of the setup of both cameras is similar and consists of an illumination system with three halogen lights (2900 K) mounted under an angle of 35 degrees, and a scanner which is used to move the sample under the camera so that it can be imaged per line. In Fig. 1, a representation of one of the cameras is shown.

Data acquisition and correlation

During the data acquisition, the specimen was considered as a cube with six resection sides and images were captured of each side, see Fig. 2. To acquire the hyperspectral images, the specimen was placed on a container tray. This tray, attached reproducibly to the translation frame of each scanner. Using this configuration, each resection side could be imaged with both cameras sequentially, without manipulating the specimen when transitioning from one camera to the other. Once imaging of one resection side was completed, the specimen was manually repositioned to ensure that the next side could be similarly imaged with both cameras in succession. To reposition the specimen manually, sutures were used that had been strategically positioned on the specimen during the surgical procedure. Surgeons and pathologists use these sutures as reference markers to determine the specimen's orientation within the patient's body (a single suture indicates the resection side facing the nipple of the breast whereas double sutures indicate the side oriented toward dorsal, i.e. the patient's back). Hence, these sutures could be used to correlate the hyperspectral images of the resection sides with the pathology results.

Data preprocessing

We performed a dark measurement to compensate for the dark current in the hyperspectral imaging systems. Secondly, we performed reference measurements on Spectralon (SRT-99-100, Labsphere, Northern Sutton, New Hampshire, USA) for both cameras to compensate for the spectral dependence of lamp output and camera sensitivity. The raw intensity hyperspectral images were converted into diffuse reflectance images, using the procedure as explained by Kho $et \, al.^{45}$. To obtain a consistent size and spatial resolution among the hyperspectral images from the VIS and NIR camera, an affine registration was employed to resize them, yielding images with a dimension of 320×256 pixels corresponding to a spatial resolution of 0.5 mm per pixel. Given that the

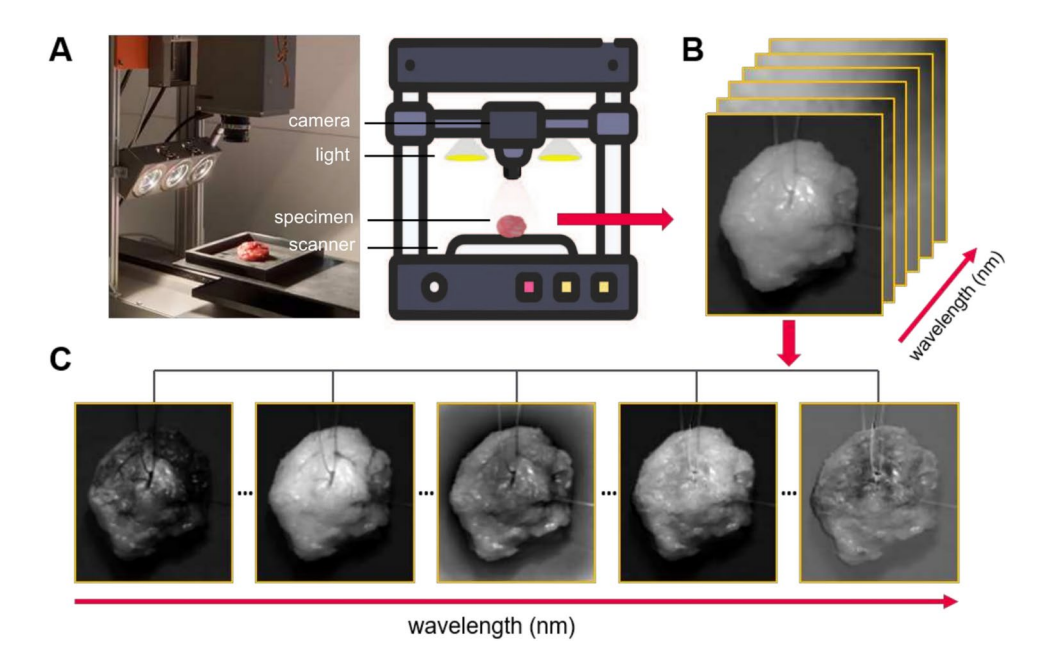


Fig. 1. Illustration of the hyperspectral imaging setup. By capturing images of the lumpectomy specimen (A), a three-dimensional array of images can be generated across a broad range of the electromagnetic spectrum (B). Five example images out of the total 528, each captured at a distinct wavelength, provide diverse spatial information about the specimen (C). Every pixel in the image also contains spectral information, offering additional details about the tissue's composition. By considering this information for multiple wavelengths, a diffuse reflectance spectrum, i.e. an optical fingerprint can be generated for each pixel which enables the detection of cancer cells.

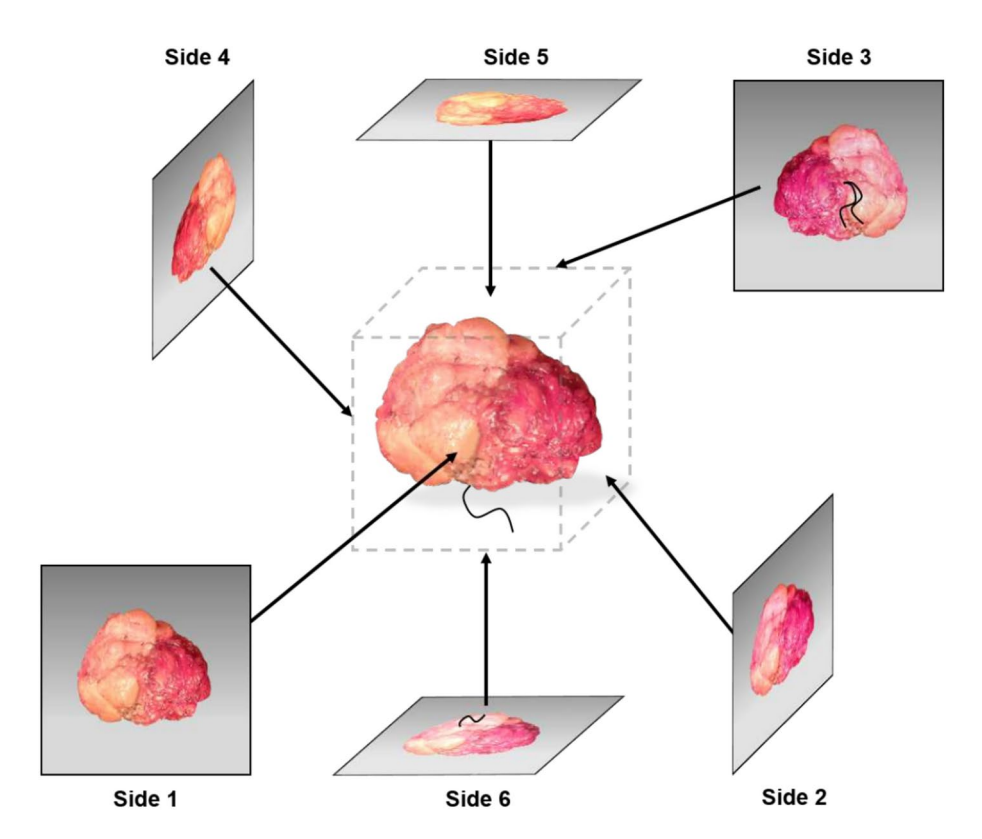


Fig. 2. Orientation of the lumpectomy specimen during data acquisition. The specimen is considered as a cube with six resection sides. To acquire hyperspectral images of the entire resection surface, each side of the specimen is imaged according to a fixed order (sides 1-6). Surgical sutures, placed during the procedure to preserve the specimen's original orientation, serve as reference markers. A single suture indicates the side facing the nipple, while double sutures indicate the side facing the dorsal (back) of the patient. These sutures allow for cross-referencing the imaged resection sides with the pathology results. Based on the suture markings, the specimen was inked and processed in the pathology department, where the surgical margin status of each side was evaluated by a pathologist.

sensors have a reduced sensitivity for wavelengths at the ends of the spectral range, these were excluded from the analysis. As a result, hyperspectral images were used with a wavelength range from 450 to 951 nm for the VIS camera (consisting of 318 wavelength bands) and from 954 to 1650 nm for the NIR camera (comprising 210 wavelength bands). Additionally, a standard normal variate (SNV) normalization was applied per camera to account for the variability between measurements due to the uneven tissue structure of the lumpectomy specimen⁶⁹. The hyperspectral images were also post-processed to exclude pixels corresponding to non-tissue-related objects, such as the tissue container tray, sutures, skin, and shadow areas. Excluding shadow areas was important because their reduced illumination affects the measurements and cannot be effectively corrected for using SNV normalization⁴⁸. The post-processing involved setting a local threshold value to identify these pixels and converting them to black background pixels.

Tissue classification

The lumpectomy dataset was divided at a patient level, with approximately 80% of patients assigned to the training set and around 20% to the test set while keeping the data of patients in one of the respective sets. The training set consisted of 332 hyperspectral measurements (i.e. SNV normalized reflectance spectra) from 168 patients that were correlated to ground-truth hematoxylin and eosin-stained (H&E) images from histopathology. For a precise pixel-level correlation between the hyperspectral measurements and ground-truth labels, black ink markers were strategically placed at the position of the hyperspectral measurements from which we intended to extract the tissue labels. These markers were subsequently identifiable on the H&E images, allowing the corresponding tissue labels (healthy or tumorous) to be accurately retrieved. For further details regarding the correlation of the hyperspectral measurements with the ground-truth labels, the reader is referred to our previous research in which we elaborate on the approach⁶⁸. Per patient, a maximum of three ink markers at one side of the lumpectomy resection surface was allowed due to regulations within the histopathology workflow. Consequently, only a limited number of spectra (pixels) from the entire resection surface could be correlated to the histology ground-truth labels.

A weighted K-Nearest Neighbors (kNN) classification algorithm was developed on the training set to discriminate healthy from tumor tissue, i.e fat and/or connective tissue from invasive carcinoma (IC) and/or carcinoma in situ (CIS), respectively. After training the classification algorithm, its performance was evaluated

using a test set consisting of hyperspectral images obtained from 36 patients. This test set included labels indicating the margin status for the entire specimen (0: negative margin, 1: positive margin). The hyperspectral images in the test set covered the entire resection surface of the lumpectomy specimen, reflecting the aim to comprehensively assess the surgical margins. In total, six images were collected per lumpectomy specimen. To determine which sides of the imaged resection surface were tumor-positive, surgical sutures were used that had been positioned on the specimen to preserve its original orientation in the patient's body, see Section *Data acquisition and correlation* and Fig. 2. Based on the sutures, it was known how the specimen would be inked in the pathology department. The ink was applied to the specimen's edges, and these inked areas were later used to match the specimen with the imaged resection sides. This allowed us to align the imaged resection sides with the corresponding sides evaluated by pathology. After imaging, the specimen was sliced and further processed at the pathology department according to standard protocol. The obtained H&E images were then evaluated by a pathologist, who assessed the surgical margins. According to the pathology reports, we were able to determine which lumpectomy specimens had a positive resection margin and identify the specific locations of these tumor-positive areas (specimen side).

Performance evaluation

Due to the lack of consensus in international oncology guidelines regarding adequate resection margins, definitions vary across countries⁷⁰. To align more broadly with these guidelines, we opted to incorporate both Dutch and USA guidelines for evaluating the diagnostic performance of our tissue classification algorithm. According to the Dutch guidelines, margins are considered tumor-positive when IC and/or CIS are detected on the inked surface of the lumpectomy specimen, commonly referred to as "tumor on ink"⁷¹. The USA guidelines define a positive margin for CIS if it is within 2 mm of the inked surface⁷². For IC, no tumor on ink is deemed an adequate margin⁷³. When adhering to the USA guidelines in our evaluation, a positive margin is identified whenever any lesion is within 2 mm of the inked surface, irrespective of its type. This is because HSI imaging can detect IC as well as CIS, but is hardly able to differentiate between both⁴⁶. Therefore, we trained and tested our algorithm to detect the presence or absence of any tumor (IC or/and CIS) within the indicated surgical margins.

We evaluated the performance of the developed classification algorithm using the sensitivity, specificity, accuracy, area under the curve (AUC) and Matthew's Correlation Coefficient (MCC) as performance metrics⁶⁸. The sensitivity, specificity and accuracy were determined based on the optimal cut-off point on the receiver operating characteristics (ROC) curve. Also, the associated 95% confidence intervals (CI) were calculated using the Clopper-Pearson interval method⁷⁴.

Results

Dataset description

Within this *ex vivo* study, the lumpectomy specimens of in total 204 female patients were examined. Table 1 gives details on the characteristics of these patients. The average age was 57 ± 11 years (mean \pm standard deviation (STD)), with most patients being post-menopausal. The majority had an early TNM stage of 1 (135 patients, 66%) or a precancerous stage of 0, i.e. CIS (37 patients, 18%). Given the American College of Radiology (ACR) score, the majority of patients had either a scattered fibroglandular (78 patients, 38%) or heterogeneously dense breast density (82 patients, 40%). Only a minority (38 patients, 19%) underwent neoadjuvant therapy. The lumpectomy specimens had an average size and mass of respectively 56 ± 55 cm³ and 26 ± 27 g (mean \pm STD).

The dataset consisted of 168 patients in the training set and 36 patients in the test set. Table 2 presents the number of tumor-positive margins in the test set. The results are based on oncology guidelines from both the Netherlands and the USA, defining positive margins as the presence of tumor tissue (including IC and/or CIS) within a distance of 0 mm and 2 mm from the inked surface, respectively. Additionally, the table provides details on cancer subvariants. For the 0 mm margin or "tumor on ink" lesions, thirteen patients had a positive resection margin, representing 36% of cases. Among these patients, there were four doubtful cases of CIS lesions (3 DCIS, 1 LCIS) where the pathologist had uncertainties regarding their radicality. With a 2 mm margin, the number of positive margins increased to eighteen patients, comprising 50% of the total.

Overall, the hyperspectral cameras required an average of 7 minutes to capture the entire resection surface of the lumpectomy specimen per patient. The tissue classification and analysis of the resection sides took on average less than 3 minutes using a computer workstation with Intel(R) Xeon(R) E-2144G CPU @ 3.60GHz and 16GB of RAM memory.

Classification lumpectomy resection surface

Fig. 3A demonstrates the ROC curves for the kNN classification algorithm, used to evaluate its performance in discriminating healthy from tumor tissue across the entire resection surface, with margins defined at 0 mm and 2 mm distance. The curves are generated using prediction scores derived from the total number of classified tumor pixels per patient. Using the optimal cut-off point on the ROC curves, the confusion matrices shown in Fig. 3B and Fig. 3C are created, illustrating the predicted versus actual number of patients with negative (healthy) or positive (tumor) margins for the 0 mm and 2 mm, respectively.

For the 0 mm margin, we achieved a sensitivity of 92% (95% CI, 0.64-1.00) and specificity of 78% (95% CI, 0.56-0.93), with an accuracy of 83% (95% CI, 0.67-0.94). The AUC and MCC were 89% and 68%, respectively. For the 2 mm margin, sensitivity and specificity were 83% (95% CI, 0.59-0.96) and 72% (95% CI, 0.47-0.90), respectively. The obtained accuracy was 78% (95% CI, 0.61-0.90), with an AUC of 85% and MCC of 56%.

In the remainder of this section, we will elaborate the results through two patient cases in detail. In Figs. 4-5 these examples are presented, showing the lumpectomy specimens from the patients along with their corresponding classification results. In both figures, the first row indicates the RGB color image of the lumpectomy resection surface imaged from all six sides (extracted from the hyperspectral data). The lumpectomy specimen

Characteristic	No. of patients (%)	Mean ± STD
Age, years		57 ± 11
< 50	52 (25)	
50-59	73 (36)	
60-69	45 (22)	
≥ 70	34 (17)	
TNM staging, pT		
0	37 (18)	
1	135 (66)	
2	30 (15)	
3	2(1)	
Menopausal stage		
Pre	44 (22)	
Peri	18 (9)	
Post	118 (58)	
Unknown	24 (12)	
Breast side		
Left	100 (49)	
Right	104 (51)	
Breast density, ACR1 score		
1	15 (7)	
2	78 (38)	
3	82 (40)	
4	24 (12)	
Unknown	5 (2)	
Neoadjuvant therapy ²		
Chemotherapy	22 (11)	
Hormone therapy	14 (7)	
Immunotherapy	2 (1)	
None	166 (81)	
Size lumpectomy, cm ³		56 ± 55
Mass lumpectomy, g		26 ± 27

Table 1. Patient characteristics ¹American college of radiology score; 1 = almost entirely fatty. 2 = scattered fibroglandular densities. 3 = heterogeneously dense. 4 = extremely dense. ²Only patients with either no or partial tumor response to neoadjuvant therapy were included.

	Margin 0 mm*		Margin 2 mm ⁺			
	No. of patients (%)	Subvariants	No. of patients (%)	Subvariants		
Cancer type						
IC	6 (17)	1 ILC, 5 IDC	8 (22)	1 ILC, 7 IDC		
CIS	7 (19)	6 DCIS, 1 LCIS	8 (22)	7 DCIS, 1 LCIS		
IC & CIS	-	-	2 (6)	2 IDC & DCIS		
	13 (36)		18 (50)			

Table 2. Number of tumor-positive margins in test set. *based on Dutch oncology guidelines. *Based on USA oncology guidelines. ILC = invasive lobular carcinoma. IDC = invasive ductal carcinoma. DCIS = ductal carcinoma in situ. LCIS = lobular carcinoma in situ.

is oriented such that the single surgical suture facing the nipple consistently appears at the bottom of all images, while the double sutures pointing toward the dorsal side are visible in side 3. The second and third row represent the probability maps generated by the kNN classification algorithm and the corresponding tissue classification maps, respectively. The probability map illustrates the predicted tumor locations on the lumpectomy resection side, with blue areas indicating a lower estimated tumor percentage and yellow areas representing a higher tumor percentage, particularly in regions likely to have a positive margin. The classification map depicts the final tissue assessment of healthy and tumor tissue per resection side, determined by applying a probability threshold value of 0.99 for tumor.

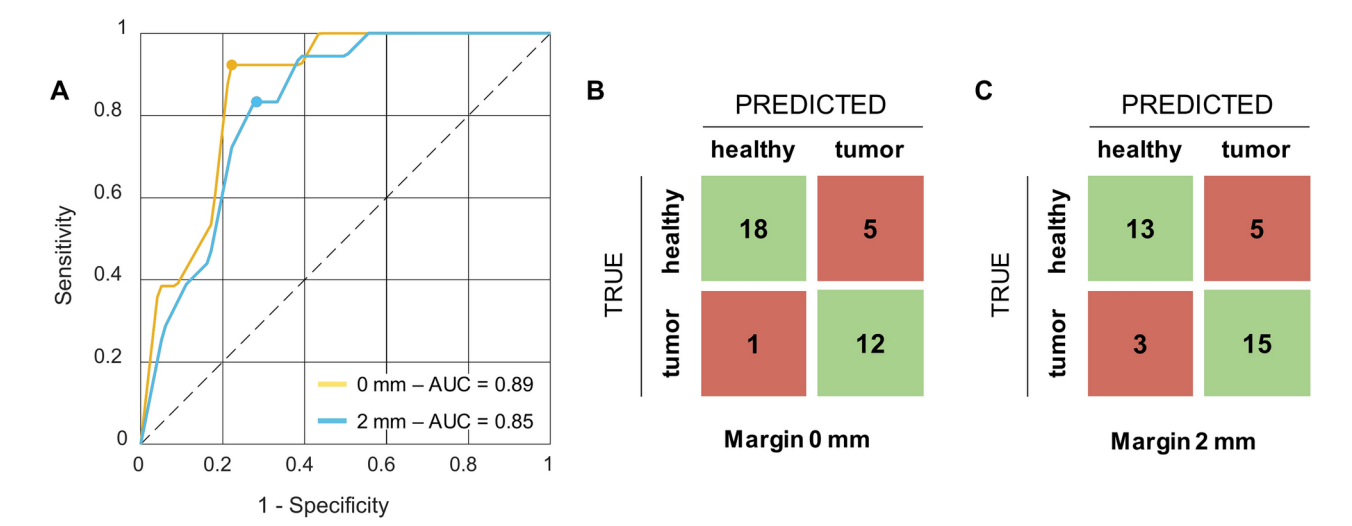


Fig. 3. Classification performance. (**A**) ROC curves of the classification algorithm to distinguish healthy tissue from tumor tissue within a margin of 0 (yellow) and 2 mm (blue) from the entire resection surface. The circular markers indicate the selected cut-off points for which the results are reported. (**B-C**) Confusion matrices based on the cut-off points on the ROC curves, showing the predicted and true number of patients with a negative (healthy) or positive (tumor) margin.

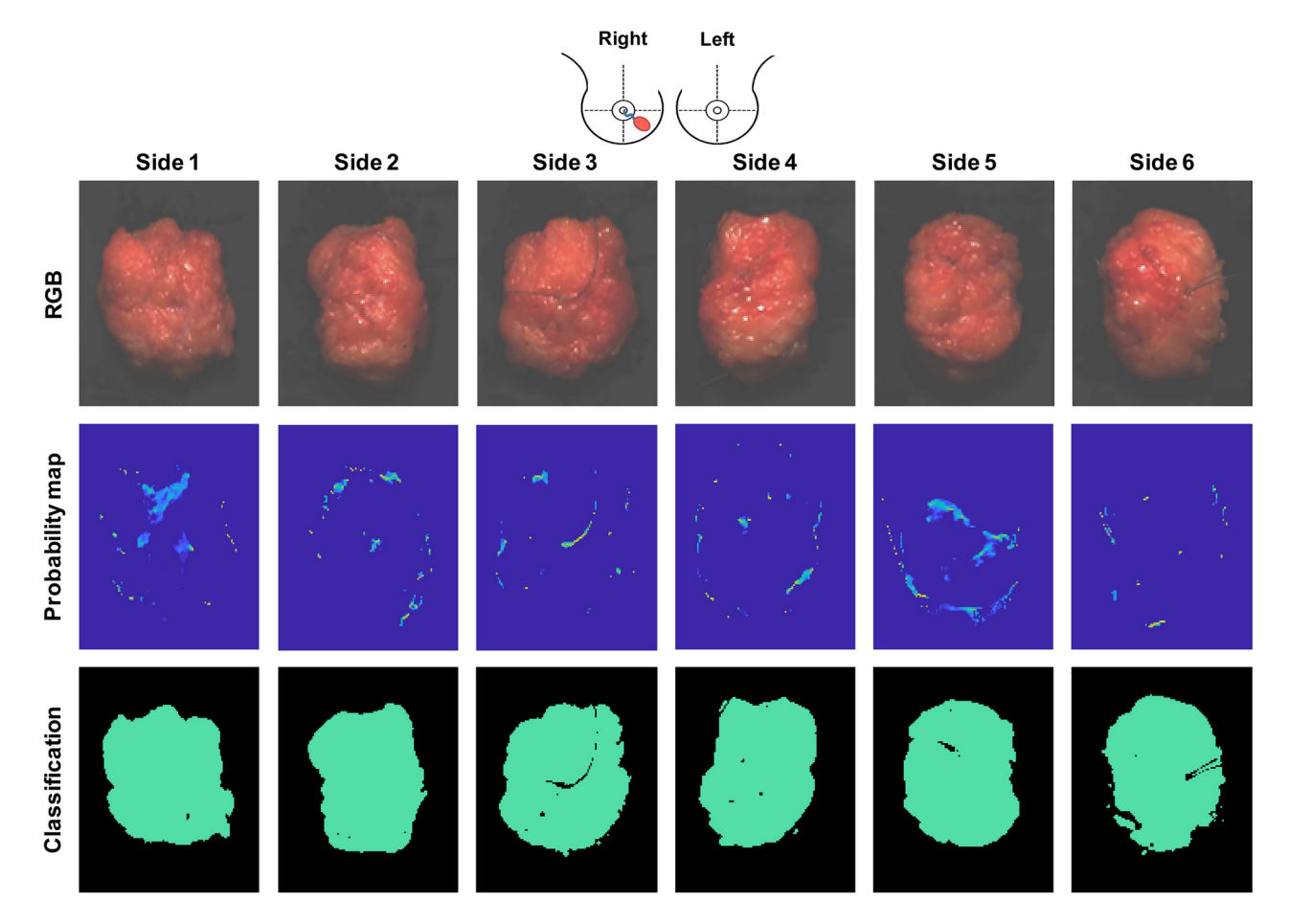


Fig. 4. Patient case 1: Lumpectomy specimen with a tumor-negative resection margin. The specimen was excised medially in the lower inner quadrant of the right breast. The six resection sides are depicted in the RGB color images, which are generated from hyperspectral data. The probability and classification map are the results of the classification algorithm for each side. Areas with a higher tumor probability are visualized in yellow while the final classification for tumor tissue is highlighted in red.

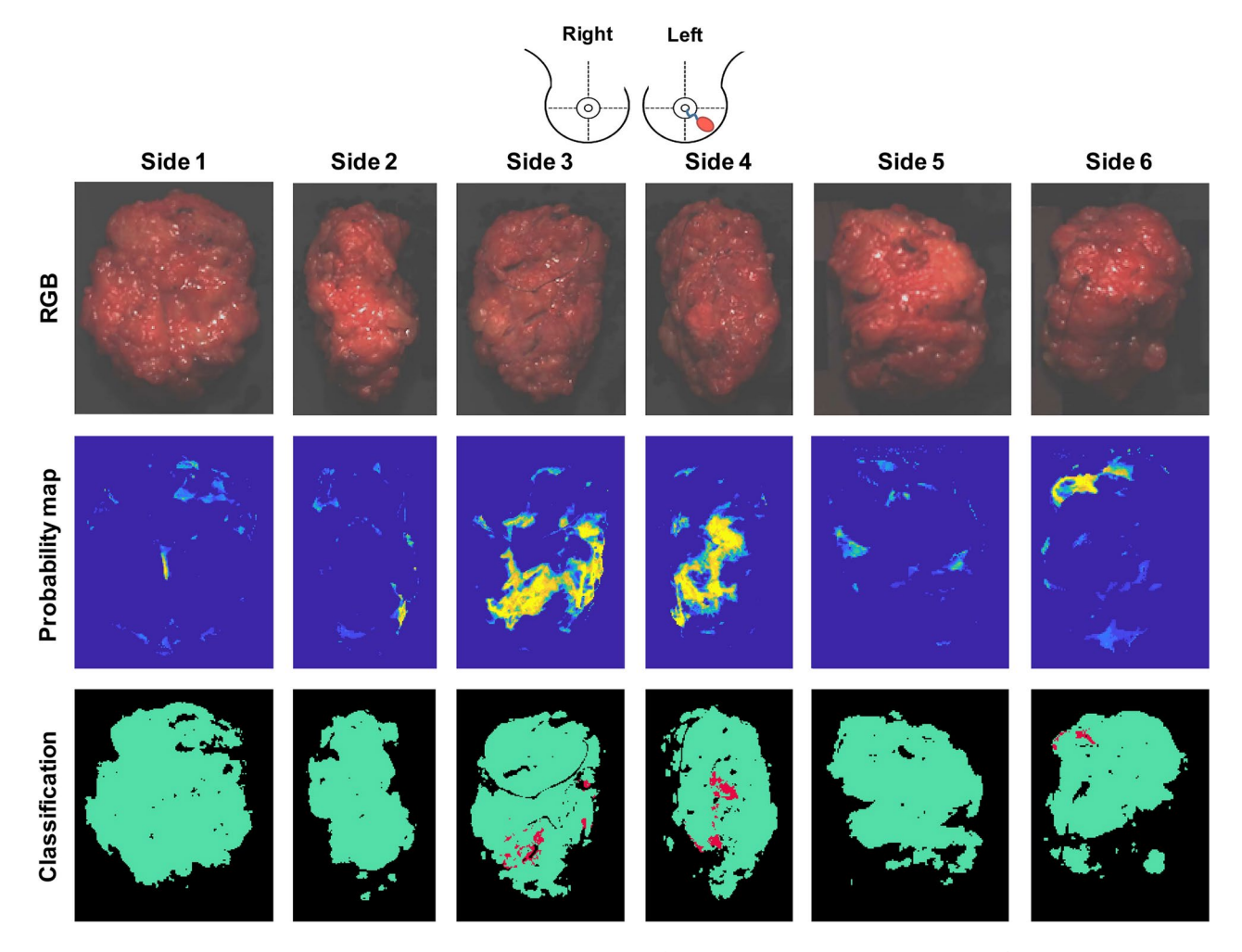


Fig. 5. Patient case 2: Lumpectomy specimen with a tumor-positive resection margin. The specimen was excised laterally in the lower outer quadrant of the left breast. The six resection sides are depicted in the RGB color images, which are generated from hyperspectral data. The probability and classification map are the results of the classification algorithm for each side. Areas with a higher tumor probability are visualized in yellow while the final classification for tumor tissue is highlighted in red.

Fig. 4 depicts an IC case (i.e. IDC) of a patient with a tumor-negative resection margin (at least 3 mm toward dorsal) as determined by histology results. The specimen was excised medially in the lower inner quadrant of the right breast. The probability maps reveal minimal areas with a high tumor percentage, and the corresponding classification maps also appear entirely green across all resection sides. This indicates a lumpectomy resection surface with clear margins for both 0 and 2 mm, confirming the pathology outcomes.

Fig. 5 represents a patient case with a tumor-positive resection margin. The lumpectomy specimen is excised from the lower outer (lateral) quadrant of the left breast. Histology results revealed a CIS (i.e. DCIS) lesion on the inked surface, at the dorsal and craniolateral sides corresponding to respectively sides 3 and 4 in the images. The classification maps highlight the lesion in red on the resection sides, aligning with the pathology findings. In side 6, the lesion is visible at the top left of the lumpectomy surface, indicating its presence at the craniolateral side from a different (nipple side) perspective. Additionally, it can be noticed that sutures and shadow areas are correctly identified and converted to black background pixels.

Discussion

In the past few years, there has been a significant improvement in the prognosis of breast cancer due to advancements in early diagnostics and effective treatment methods including BCS. A positive patient outcome after BCS depends on the real-time assessment of the lumpectomy's resection surface during surgery but despite the critical need for an adequate intraoperative margin assessment technique, surgeons still have to rely on the time-consuming gold standard of histopathology. Consequently, the challenge of inadequate surgical margins persists, necessitating additional treatment for residual tumors to reduce the risk of local recurrence. In this study, we have employed HSI as a margin assessment technique to distinguish between healthy and tumor tissue on the resection surface of lumpectomy specimens, aiming to overcome this clinical need. With the encouraging results of this study we have successfully demonstrated that by applying HSI with our developed classification

algorithm, the entire lumpectomy's resection surface following BCS can be assessed within a short timeframe of 10 minutes with a high diagnostic performance. Thereby we have made a major step toward the clinical implementation of HSI in the surgical workflow.

We achieved a sensitivity of 92% for identifying patients with a tumor-positive resection margin at the 0 mm margin distance. This indicates that we accurately identified nearly all patients in our test set with a tumor-positive tissue label, with only one patient missed. At the 2 mm margin distance, our sensitivity was 83%, indicating three missed patients. Upon closer examination of these false-negative cases (including the patient missed at the 0 mm margin), histopathology revealed that the missed tumors either consisted solely of residual tumor isles or were smaller than 2 mm in width. These findings are consistent with previous results that indicate reduced classification accuracy of HSI for tumors smaller than 3×3 mm⁴⁵. According to Dutch oncology guidelines, these cases would not necessitate re-excision since the requirement is a minimal width of 4 mm⁷¹. Instead, further treatment options such as adjuvant radiotherapy would be considered for the patient. Irrespective of the tumor size, to ensure the identification of all patients with a positive margin in an intraoperative setting, adjustments to the ROC curve's cut-off point can be made (Fig. 3A). For instance, increasing sensitivity to 94% on the ROC at the 2 mm margin may decrease specificity to 61%. This adjustment improves tumor detection rates but also increases the likelihood of classifying healthy tissue as suspicious, potentially leading to unnecessary excision of healthy tissue. However, even with the excision of some extra tissue, it remains preferable to avoid a positive margin.

In this study, we have treated the lumpectomy specimen as a cube with six distinct resection sides to ensure consistent and reproducible data acquisition and analysis. However, in practice, the specimen tends to have a more spherical shape lacking clearly defined corners, despite the distinct depiction of corners in hyperspectral images. This discrepancy can lead to inaccuracies in correlating with pathology reports, particularly when identifying a positive margin at image transitions. The tissue's surface inclination may result in shadow areas that affect reflectance spectra, requiring their exclusion from the analysis 48. Additionally, the tissue may overlap in the images. Consequently, determining which hyperspectral images align with this tumor-positive tissue label can be challenging. Since the accuracy of the correlation between ground-truth labels and images plays a major role in the performance of the classification algorithm, we addressed this in the test set by assigning for each patient with a positive margin, tumor-positive labels to the entire lumpectomy specimen rather than individually for each imaged side of the specimen.

Surgical sutures on the lumpectomy specimen enable pathologists and histopathologists to determine its original position in the patient's body. This allows for routine processing and examination according to standard histopathological procedure. Furthermore, the sutures facilitate a systematic data acquisition with HSI by indicating the anatomical side of the specimen in each image (Fig. 2). This systematic approach enabled us to verify whether the classified tumor lesions accurately matched their positions on the resection surface, as indicated by pathology reports. In all cases, the lesion positions were confirmed. This indicates that if HSI would be employed during surgery, it could reveal the location of the positive margin, enabling the surgeon to identify the areas where additional resection is needed. An alternative method for confirming tumor lesion positions would involve placing ink markers for precise localization on the H&E images. However, during the data acquisition phase, the classification algorithm was not yet developed, preventing us from employing this method. Nevertheless, this approach has limitations, as the routine histopathology workflow allows for only a few ink mark locations to be investigated, thereby not covering the entire resection surface.

Our classification algorithm was developed to differentiate between healthy and tumor tissue on the resection surface, without distinguishing between IC, CIS, or their subvariants. While the primary goal is to detect positive resection margins, differentiating between cancer and precursor variants can be helpful in deciding when reexcision is necessary. However, there is currently no international consensus on the definitions of positive margins and re-excisions. Oncology guidelines, which specify which cancer (sub)variants are considered tumor-positive and require re-excision, can vary from country to country. In our study, we therefore aimed to align more broadly with guidelines by adhering as closely as possible to both Dutch and USA oncology standards. Nevertheless, it is important to note that prior to surgery, information about the cancer type, size, and grade is often available from pathology biopsies and/or preoperative medical imaging. This information can be used in the decision-making process to perform a re-excision when a lesion is classified as tumor-positive.

Numerous studies have previously explored the potential of HSI as a technique for assessing resection margins in cancer surgery^{42–66}. While these studies have shown promising results, bridging the gap between their current stage and the ultimate goal of clinical implementation remains challenging. Many of these studies were in their early research phases and conducted under controlled conditions that may not accurately represent real surgical environments. The difficulty of conducting research within surgical settings contributes to a scarcity of clinically labeled datasets. In our study, we have demonstrated the efficacy of hyperspectral imaging in quickly evaluating the entire resection surface of ex vivo lumpectomy specimens. As such, this study represents the first of its kind in this regard, aiming to advance the application of HSI for margin assessment with the ultimate objective of achieving clinical implementation.

Compared to other technologies, hyperspectral imaging provides a fast, automated, and non-contact solution for intraoperative margin assessment. Unlike Raman spectroscopy or fluorescence imaging, which rely on contrast agents or complex spectral interpretation, HSI offers label-free imaging while capturing detailed spectral data from the entire tissue surface. Furthermore, our approach enables real-time full-margin evaluation, making it significantly faster than traditional histopathology and frozen section analysis, which can take anywhere from 30 minutes to several days while assessing only limited portions of the margin.

In summary, we have shown that combining hyperspectral imaging with our classification algorithm achieves high diagnostic performance, effectively distinguishing between healthy and tumor tissue within the resection margins of lumpectomy specimens. This achievement represents a major advancement toward providing real-

time feedback to surgeons during breast-conserving surgery in order to improve the accuracy of surgical margin assessment, particularly in complex cases where precise tumor identification is challenging. This advancement is important for better patient outcomes and reducing the burden of additional treatments for residual tumors.

For successful integration into the surgical workflow, it is essential to ensure that the classification algorithm is both robust and adaptable across different clinical conditions. By training the algorithm on data obtained directly from the original resection surface of lumpectomy specimens, we ensured that it was exposed to unprocessed tissue with a consistent surface structure. Although the data was collected ex vivo, measurements were performed immediately after surgery to minimize the effects of tissue degradation. Moreover, a previous study reported no significant differences in optical properties between ex vivo and in vivo tissue data, implying that the algorithm may be applicable in both settings⁷⁵. However, further investigation is necessary to confirm these findings and evaluate potential variability across different clinical conditions. To further enhance real-time applicability, future efforts could focus on the development of more compact camera setups, such as dedicated snapshot hyperspectral cameras, for close proximity to the patient. Currently, commercial models offer faster data capture than current line-scanning models, with speeds exceeding 20 fps, making real-time feedback on in vivo tissue during breast-conserving surgery possible. However, their limited number of wavelengths presents a challenge. Before HSI can be fully implemented in clinical practice, further investigation is needed to understand how the reduced wavelength range impacts classification performance compared to broader spectral data. Addressing this is crucial for ensuring the feasibility and accuracy of real-time surgical margin assessment.

Beyond technical considerations, the successful adoption of HSI in surgery will depend on cost-effectiveness, accessibility, and surgeon training. Initial system costs and the need for specialized training could pose barriers to widespread adoption. Therefore, further studies should focus on evaluating the cost-benefit ratio of HSI in reducing re-excision rates and improving surgical outcomes. Additionally, user training programs and simplified interfaces will be crucial to ensure that surgeons and operating room staff can efficiently integrate HSI into their workflow. By addressing these challenges and leveraging ongoing advancements in HSI technology, this imaging modality has the potential to become a practical and valuable tool for intraoperative decision-making in breast-conserving surgery and beyond.

Data availability

The datasets generated during and/or analysed during the current study are not publicly available due to privacy or ethical restrictions but are available from the corresponding author on reasonable request.

Received: 2 December 2024; Accepted: 14 March 2025

Published online: 20 March 2025

References

- 1. Sung, H. et al. Global cancer statistics 2020: Globocan estimates of incidence and mortality worldwide for 36 cancers in 185 countries. CA: a cancer journal for clinicians 71, 209–249 (2021).
- O'Kelly Priddy, C. M., Forte, V. A. & Lang, J. E. The importance of surgical margins in breast cancer. *Journal of surgical oncology* 113, 256–263 (2016).
- 3. McCahill, L. E. et al. Variability in reexcision following breast conservation surgery. Jama 307, 467-475 (2012).
- 4. Waljee, J. F., Hu, E. S., Newman, L. A. & Alderman, A. K. Predictors of re-excision among women undergoing breast-conserving surgery for cancer. *Annals of surgical oncology* 15, 1297–1303 (2008).
- 5. Aziz, D. et al. The role of reexcision for positive margins in optimizing local disease control after breast-conserving surgery for cancer. *The breast journal* 12, 331–337 (2006).
- Esbona, K., Li, Z. & Wilke, L. G. Intraoperative imprint cytology and frozen section pathology for margin assessment in breast conservation surgery: a systematic review. *Annals of surgical oncology* 19, 3236–3245 (2012).
- Langhans, L. et al. Reoperation rates in ductal carcinoma in situ vs invasive breast cancer after wire-guided breast-conserving surgery. JAMA surgery 152, 378–384 (2017).
- 8. Merrill, A. L. et al. Implications of new lumpectomy margin guidelines for breast-conserving surgery: changes in reexcision rates and predicted rates of residual tumor. *Annals of surgical oncology* 23, 729–734 (2016).
- 9. Merrill, A. L. et al. Should new "no ink on tumor" lumpectomy margin guidelines be applied to ductal carcinoma in situ (dcis)? a retrospective review using shaved cavity margins. *Annals of surgical oncology* 23, 3453–3458 (2016).
- 10. Alrahbi, S. et al. Extent of margin involvement, lymphovascular invasion, and extensive intraductal component predict for residual disease after wide local excision for breast cancer. Clinical Breast Cancer 15, 219–226 (2015).
- 11. Landercasper, J. et al. A community breast center report card determined by participation in the national quality measures for breast centers program. *The breast journal* **16**, 472–480 (2010).
- 12. Van Den Bruele, A. B., Jasra, B., Smotherman, C., Crandall, M. & Samiian, L. Cost-effectiveness of surgeon performed intraoperative specimen ink in breast conservation surgery. *Journal of Surgical Research* 231, 441–447 (2018).
- Pradipta, A. R. et al. Emerging technologies for real-time intraoperative margin assessment in future breast-conserving surgery. Advanced science 7, 1901519 (2020).
- 14. Aref, M. H. F. et al. Low-cost commercial integrated spectral sensor for revealing breast cancer margins. In 2024 14th International Conference on Electrical Engineering (ICEENG), 137–141 (IEEE, 2024).
- 15. MOSCHETTA, M. et al. Role of specimen us for predicting resection margin status in breast conserving therapy. *Il Giornale di Chirurgia-Journal of the Italian Surgical Association* **36**, 201–204 (2015).
- Veluponnar, D. et al. Toward intraoperative margin assessment using a deep learning-based approach for automatic tumor segmentation in breast lumpectomy ultrasound images. Cancers 15, 1652 (2023).
- 17. Schnabel, F. et al. A randomized prospective study of lumpectomy margin assessment with use of marginprobe in patients with nonpalpable breast malignancies. *Annals of surgical oncology* **21**, 1589–1595 (2014).
- Thill, M., Röder, K., Diedrich, K. & Dittmer, C. Intraoperative assessment of surgical margins during breast conserving surgery of ductal carcinoma in situ by use of radiofrequency spectroscopy. *The Breast* 20, 579–580 (2011).
 Pappo, I. et al. Diagnostic performance of a novel device for real-time margin assessment in lumpectomy specimens. *Journal of*
- Surgical Research 160, 277–281 (2010).

 20. Kupstas, A. et al. A novel modality for intraoperative margin assessment and its impact on re-excision rates in breast conserving
- 20. Kupstas, A. et al. A novel modality for intraoperative margin assessment and its impact on re-excision rates in breast conserving surgery. *The American Journal of Surgery* **215**, 400–403 (2018).

- 21. Dixon, J. M. et al. Intra-operative assessment of excised breast tumour margins using clearedge imaging device. *European Journal of Surgical Oncology (EJSO)* 42, 1834–1840 (2016).
- Shipp, D. W. et al. Intra-operative spectroscopic assessment of surgical margins during breast conserving surgery. Breast Cancer Research 20, 1–14 (2018).
- 23. Haka, A. S. et al. Diagnosing breast cancer using raman spectroscopy: prospective analysis. *Journal of biomedical optics* **14**, 054023 (2009).
- 24. Thomas, G. et al. Evaluating feasibility of an automated 3-dimensional scanner using raman spectroscopy for intraoperative breast margin assessment. *Scientific reports* 7, 1–14 (2017).
- 25. Veluponnar, D. et al. Diffuse reflectance spectroscopy for accurate margin assessment in breast-conserving surgeries: importance of an optimal number of fibers. *Biomedical optics express* 14, 4017–4036 (2023).
- Veluponnar, D. et al. Margin assessment during breast conserving surgery using diffuse reflectance spectroscopy. Journal of biomedical optics 29, 045006–045006 (2024).
- Park, K. U. et al. Digital breast tomosynthesis for intraoperative margin assessment during breast-conserving surgery. Annals of surgical oncology 26, 1720–1728 (2019).
- 28. Pleijhuis, R. et al. Near-infrared fluorescence (nirf) imaging in breast-conserving surgery: assessing intraoperative techniques in tissue-simulating breast phantoms. *European Journal of Surgical Oncology (EJSO)* 37, 32–39 (2011).
- 29. Qiu, S.-Q. et al. Micro-computed tomography (micro-ct) for intraoperative surgical margin assessment of breast cancer: a feasibility study in breast conserving surgery. European Journal of Surgical Oncology 44, 1708–1713 (2018).
- 30. Zysk, A. M. et al. Intraoperative assessment of final margins with a handheld optical imaging probe during breast-conserving surgery may reduce the reoperation rate: results of a multicenter study. *Annals of surgical oncology* 22, 3356–3362 (2015).
- Ha, R. et al. Optical coherence tomography: a novel imaging method for post-lumpectomy breast margin assessment-a multireader study. Academic radiology 25, 279–287 (2018).
- 32. Foo, K. Y. et al. Optical palpation for tumor margin assessment in breast-conserving surgery. *Biomedical Optics Express* 12, 1666–1682 (2021).
- Fereidouni, F. et al. Microscopy with ultraviolet surface excitation for rapid slide-free histology. Nature biomedical engineering 1, 957–966 (2017).
- 34. Wong, T. T. et al. Fast label-free multilayered histology-like imaging of human breast cancer by photoacoustic microscopy. *Science advances* 3, e1602168 (2017).
- 35. Li, R. et al. Assessing breast tumor margin by multispectral photoacoustic tomography. *Biomedical optics express* 6, 1273–1281
- Vartholomatos, G. et al. Rapid assessment of resection margins during breast conserving surgery using intraoperative flow cytometry. Clinical Breast Cancer 21, e602–e610 (2021).
- Khoobehi, B., Beach, J. M. & Kawano, H. Hyperspectral imaging for measurement of oxygen saturation in the optic nerve head. Investigative ophthalmology & visual science 45, 1464–1472 (2004).
- 38. Mordant, D. et al. Oxygen saturation measurements of the retinal vasculature in treated asymmetrical primary open-angle glaucoma using hyperspectral imaging. Eye 28, 1190–1200 (2014).
- Johnson, W. R., Wilson, D. W., Fink, W., Humayun, M. & Bearman, G. Snapshot hyperspectral imaging in ophthalmology. *Journal of biomedical optics* 12, 014036–014036 (2007).
- Akbari, H., Kosugi, Y., Kojima, K. & Tanaka, N. Blood vessel detection and artery-vein differentiation using hyperspectral imaging. In 2009 Annual International Conference of the IEEE Engineering in Medicine and Biology Society, 1461–1464 (IEEE, 2009).
- 41. Akbari, H., Kosugi, Y., Kojima, K. & Tanaka, N. Detection and analysis of the intestinal ischemia using visible and invisible
- hyperspectral imaging. *IEEE Transactions on Biomedical Engineering* **57**, 2011–2017 (2010).

 42. Ravì, D., Fabelo, H., Callic, G. M. & Yang, G.-Z. Manifold embedding and semantic segmentation for intraoperative guidance with hyperspectral brain imaging. *IEEE transactions on medical imaging* **36**, 1845–1857 (2017).
- 43. Fabelo, H. et al. Spatio-spectral classification of hyperspectral images for brain cancer detection during surgical operations. *PloS one* 13, e0193721 (2018).
- 44. Fabelo, H. et al. Deep learning-based framework for in vivo identification of glioblastoma tumor using hyperspectral images of human brain. *Sensors* 19, 920 (2019).
- 45. Kho, E. et al. Hyperspectral imaging for resection margin assessment during cancer surgery. *Clinical cancer research* **25**, 3572–3580 (2019)
- 46. Kho, E. et al. Broadband hyperspectral imaging for breast tumor detection using spectral and spatial information. *Biomedical optics express* 10, 4496–4515 (2019).
- 47. Aboughaleb, I. H., Aref, M. H. & El-Sharkawy, Y. H. Hyperspectral imaging for diagnosis and detection of ex-vivo breast cancer. *Photodiagnosis and Photodynamic Therapy* 31, 101922 (2020).
- 48. Kho, E. et al. Feasibility of ex vivo margin assessment with hyperspectral imaging during breast-conserving surgery: From imaging tissue slices to imaging lumpectomy specimen. *Applied Sciences* 11, 8881 (2021).
- Baltussen, E. J. et al. Hyperspectral imaging for tissue classification, a way toward smart laparoscopic colorectal surgery. *Journal of biomedical optics* 24, 016002 (2019).
- 50. Manni, F. et al. Hyperspectral imaging for colon cancer classification in surgical specimens: Towards optical biopsy during image-guided surgery. In 2020 42nd Annual International Conference of the IEEE Engineering in Medicine & Biology Society (EMBC), 1169, 1173 (IEEE 2020)
- 51. Jansen-Winkeln, B. et al. Feedforward artificial neural network-based colorectal cancer detection using hyperspectral imaging: a step towards automatic optical biopsy. *Cancers* 13, 967 (2021).
- Collins, T. et al. Automatic recognition of colon and esophagogastric cancer with machine learning and hyperspectral imaging. diagnostics 2021; 11: 1810.
- 53. Collins, T. et al. Automatic optical biopsy for colorectal cancer using hyperspectral imaging and artificial neural networks. Surgical Endoscopy 36, 8549–8559 (2022).
- 54. Liu, N., Guo, Y., Jiang, H. & Yi, W. Gastric cancer diagnosis using hyperspectral imaging with principal component analysis and spectral angle mapper. *Journal of Biomedical Optics* 25, 066005–066005 (2020).
- 55. Mitsui, T. et al. Evaluating the identification of the extent of gastric cancer by over-1000 nm near-infrared hyperspectral imaging using surgical specimens. *Journal of Biomedical Optics* 28, 086001–086001 (2023).
- Fei, B. et al. Label-free reflectance hyperspectral imaging for tumor margin assessment: a pilot study on surgical specimens of cancer patients. *Journal of biomedical optics* 22, 086009–086009 (2017).
- 57. Halicek, M. et al. Deep convolutional neural networks for classifying head and neck cancer using hyperspectral imaging. *Journal of biomedical optics* 22, 060503–060503 (2017).
- 58. Lu, G. et al. Detection of head and neck cancer in surgical specimens using quantitative hyperspectral imaginghyperspectral imaging for head and neck cancer detection. *Clinical Cancer Research* 23, 5426–5436 (2017).
- 59. Halicek, M. et al. Tumor margin classification of head and neck cancer using hyperspectral imaging and convolutional neural networks. In *Medical Imaging 2018: Image-Guided Procedures, Robotic Interventions, and Modeling*, vol. 10576, 17–27 (SPIE, 2018).
- Halicek, M. et al. Hyperspectral imaging of head and neck squamous cell carcinoma for cancer margin detection in surgical specimens from 102 patients using deep learning. Cancers 11, doi:10.3390/cancers11091367 (2019).

- 61. Weijtmans, P. J. C., Shan, C., Tan, T., De Koning, S. B. & Ruers, T. J. M. A dual stream network for tumor detection in hyperspectral images. In 2019 IEEE 16th International Symposium on Biomedical Imaging (ISBI 2019), 1256–1259 (IEEE, 2019).
- 62. Brouwer de Koning, S. G. et al. Toward assessment of resection margins using hyperspectral diffuse reflection imaging (400–1,700 nm) during tongue cancer surgery. *Lasers in surgery and medicine* **52**, 496–502 (2019).
- 63. Halicek, M., Little, J. V., Wang, X., Chen, A. Y. & Fei, B. Optical biopsy of head and neck cancer using hyperspectral imaging and convolutional neural networks. *Journal of biomedical optics* 24, 036007–036007 (2019).
- 64. Manni, F. et al. Hyperspectral imaging for glioblastoma surgery: Improving tumor identification using a deep spectral-spatial approach. Sensors 20, 6955 (2020).
- 65. Trajanovski, S., Shan, C., Weijtmans, P. J., de Koning, S. G. B. & Ruers, T. J. Tongue tumor detection in hyperspectral images using deep learning semantic segmentation. *IEEE transactions on biomedical engineering* 68, 1330–1340 (2020).
- 66. van Vliet-Pérez, S. M. et al. Hyperspectral imaging for tissue classification after advanced stage ovarian cancer surgery-a pilot study. *Cancers* 14, 1422 (2022).
- 67. Jong, L.-J.S. et al. Discriminating healthy from tumor tissue in breast lumpectomy specimens using deep learning-based hyperspectral imaging. *Biomedical optics express* 13, 2581–2604 (2022).
- 68. Jong, L.-J.S. et al. Tissue classification of breast cancer by hyperspectral unmixing. Cancers 15, 2679 (2023).
- 69. Witteveen, M. et al. Comparison of preprocessing techniques to reduce nontissue-related variations in hyperspectral reflectance imaging. *Journal of biomedical optics* 27, 106003–106003 (2022).
- 70. de Koning, S. G. B., Peeters, M.-J.T.V., Jóźwiak, K., Bhairosing, P. A. & Ruers, T. J. Tumor resection margin definitions in breast-conserving surgery: systematic review and meta-analysis of the current literature. *Clinical breast cancer* 18, e595–e600 (2018).
- kankercentrum Nederland, I. Nationaal Borstkanker Overleg Nederland, richtlijn mammacarcinoom. https://richtlijnen.nhg.org/multidisciplinaire-richtlijnen/mammacarcinoom (2012). [Online; accessed 19-December-2023].
- 72. Morrow, M. et al. Society of Surgical Oncology-American Society for Radiation Oncology-American Society of Clinical Oncology Consensus Guideline on Margins for Breast-Conserving Surgery With Whole-Breast Irradiation in Ductal Carcinoma in Situ. *Practical Radiation Oncology* 6, 287–295. https://doi.org/10.1016/j.prro.2016.06.011 (2016).
- 73. Moran, M. S. et al. Society of surgical oncology-american society for radiation oncology consensus guideline on margins for breast-conserving surgery with whole-breast irradiation in stages i and ii invasive breast cancer. *Journal of Clinical Oncology* 32, 1507–1515 (2014).
- 74. Clopper, C. J. & Pearson, E. S. The use of confidence or fiducial limits illustrated in the case of the binomial. *Biometrika* 26, 404–413 (1934).
- 75. De Boer, L. L. et al. Using drs during breast conserving surgery: identifying robust optical parameters and influence of inter-patient variation. *Biomedical optics express* 7, 5188–5200 (2016).

Acknowledgements

The authors thank the surgeons and nurses from the department of Surgery for their valuable contributions in providing the lumpectomy specimens. Additionally, they thank the NKI-AVL core Facility Molecular Pathology & Biobanking (CFMPB) for supplying NKI-AVL biobank material, and the pathologists as well as the pathologist assistants from the department of Pathology for their assistance in investigating the specimens.

Author contributions

The project was conceptualized by Lynn-Jade S. Jong, Henricus J.C.M. Sterenborg, Behdad Dashtbozorg, and Theo J.M. Ruers, with surgeries performed by Marie-Jeanne T.F.D. Vrancken Peeters and Frederieke van Duijnhoven. Experiments and investigations were conducted by Lynn-Jade S. Jong, Dinusha Veluponnar, Freija Geldof, Joyce Sanders and Marcos Da Silva Guimaraes. Data analysis and writing of the original draft was carried out by Lynn-Jade S. Jong and Behdad Dashtbozorg, while all authors participated in the review and editing process. Henricus J.C.M. Sterenborg and Theo J.M. Ruers obtained funding for the project. All authors reviewed and approved the final manuscript.

Funding

This research was funded by the Dutch Cancer Society, grant number 10747.

Declarations

Competing interests

The authors declare no competing interests.

Additional information

Correspondence and requests for materials should be addressed to B.D.

Reprints and permissions information is available at www.nature.com/reprints.

Publisher's note Springer Nature remains neutral with regard to jurisdictional claims in published maps and institutional affiliations.

Open Access This article is licensed under a Creative Commons Attribution-NonCommercial-NoDerivatives 4.0 International License, which permits any non-commercial use, sharing, distribution and reproduction in any medium or format, as long as you give appropriate credit to the original author(s) and the source, provide a link to the Creative Commons licence, and indicate if you modified the licensed material. You do not have permission under this licence to share adapted material derived from this article or parts of it. The images or other third party material in this article are included in the article's Creative Commons licence, unless indicated otherwise in a credit line to the material. If material is not included in the article's Creative Commons licence and your intended use is not permitted by statutory regulation or exceeds the permitted use, you will need to obtain permission directly from the copyright holder. To view a copy of this licence, visit https://creativecommons.org/licenses/by-nc-nd/4.0/.

© The Author(s) 2025